Design and Operation of a Droplet Deposition System for Freeform Fabrication of Metal Parts

A. A. Tseng
Fellow ASME
e-mail: ampere.tseng@asu.edu

M. H. Lee

B. Zhao

Department of Mechanical
and Aerospace Engineering,
Arizona State University,
Tempe, AZ 85287-5106

A droplet generator has been designed and built to make wax and tin alloy droplets for freeform fabrication. The linear stability theory of liquid jets for forming droplets is first reviewed. The analytical formula for predicting droplet size and breakup length at optimal conditions are then developed. The suitability of the formulas to be used for the present droplet deposition system is studied by comparing its prediction with the more accurate numerical results and previously published experimental data. Only the suitable formulation is adopted for the design and operation of the droplet generator system. Experiments have been conducted at a wide range of operating conditions including different nozzle sizes, jet velocities, and frequencies. Good agreements are found between the predictions based on the adopted analytical formulation and the experimental results. It has been found that using the present design and procedure recommended, the droplet sizes can be controlled having a size deviation of less than 3 percent and the shape variation of the deposited layer can be managed within 3 percent of its deposited width.
[DOI: 10.1115/1.1286187]

Keywords: Droplet Deposition, Droplet Formation, Free Form Fabrication, Jet Stability, Soldering Alloy, Wax

Introduction

The solid freeform fabrication technique, also known as the rapid prototyping technology, does not require preformed mandrels or tooling, instead it builds physical objects directly from computer graphical data (Jacobs [1], Beaman et al. [2]). Although the freeform fabrication technologies have been greatly advanced to fabricate complex structures, most of the commercially available freeform fabrication equipment can only process materials at relatively modest temperatures, with almost all prototyped parts made of low-temperature polymeric or oligomeric hydrocarbon materials. These low-melting temperature materials have only moderate strength and applications. For many engineering applications, however, the strength of the prototypings is critical.

In the present study, a droplet deposition system has been designed with the goal for freeforming three-dimensional metal parts to satisfy the strength requirement. The droplet deposition technique has emerged as one of the major freeform fabrication technologies for making polymer and metal parts (Orme et al. [3], Beaman et al. [2]). The system uses a technique similar to ink-jet printing (Kuhn and Myers [4]) to deposit microscopic droplets of molten metals instead of liquid ink onto the substrate. The three-dimensional physical parts can be built directly from a computerized virtual model. The computer model slices the geometric description of the part into layers and generates the contours of each layer. The contours are then discretized into points or units that represent the locations for each droplet to be deposited. Parts can be built layer by layer as the system is guided by the slicing information until they are completed.

In the present study, two types of jets are considered: one for the building material and the other for the complementary material. During processing, the building material droplet is only deposited to the location where the object is to be formed. Then a low-melting-temperature complementary material is deposited adjacent to the building materials to serve as a support structure during forming. In this manner, layers of materials form a block of solidified droplets of building and complementary materials. Since the complementary material has a much lower melting temperature, it can be easily removed after completing the deposition process, leaving only the fabricated part. In the present study, a tin-antimony (soldering) alloy is chosen for the building material while a wax is selected for the complementary material.

The accuracy of a part to be built is highly dependent on the ability to control the accuracy of the building unit, the droplet. In fact, the size of the droplet is the dominating factor in the accuracy of the final geometry and surface finish. The inherent dimensional error in droplet deposition, known as the stair-step or aliasing effect, is caused by approximating curved surfaces with stacked layers of deposited droplets. Aliasing can be alleviated if very small droplets are used although the fabrication or deposition time will increase accordingly. As a result, the ability to control the size of a droplet and its uniformity, as well as the stability during deposition, are important in freeforming the metal part.

The droplet deposition technique can also be used to produce soldering droplets for electronic packaging, including flip-chip assembly (Wallace [5]), ball grid array (BGA) packaging (Lau [6]), and fine-line printed circuit boards (Hayes et al. [7]). For those applications, the uniformity of the droplets or microballs and the accuracy of their landing location become critical and directly affects the reliability of the solder joints (Ju et al. [8]). Some feedback systems have been developed to control the uniformity of the droplet sizes (Lovelady and Watts [9]). In the present study, the uniformity of the droplets produced will be specifically evaluated as a quantitative measure of the superiority of the droplet deposition system presently developed. If the droplet uniformity and landing accuracy produced by the present system satisfy the requirements of electronic packaging, the sophisticated and expensive feedback control system becomes unnecessary.

In the present paper, optimal operating conditions for generating a wide range of droplet sizes and materials are analyzed based on the linear stability theory. The environmental effects are specifically included in the analysis. Design considerations for generating optimal droplet size and break-up length for various materials are then discussed. A laboratory scale of a freeform

Contributed by the Materials Division for publication in the JOURNAL OF ENGINEERING MATERIALS AND TECHNOLOGY. Manuscript received by the Materials Division May 5, 1999; revised manuscript received November 23, 1999, Associate Technical Editor: A. M. Rajendran.

fabrication system has been designed and built accordingly. Experiments for the generation of wax and tin-alloy droplets have been conducted in the laboratory system to verify the theoretical formulation recommended in the present study. The flying trajectory and landing position of the droplets and the quality of the deposited layer are also examined.

Stability Theory

Droplet deposition is generated using the familiar Rayleigh type of droplet generator, in which a laminar liquid jet is excited at a given frequency to break the liquid column into a series of uniform droplets (Lee [10], Kuhn and Mayers [4], Chun and Passow [11]). Normally, a piezoelectric vibrator is used to provide the exact frequency required for precise control of the droplet size. A schematic of the droplet deposition system used for the present study is shown in Fig. 1.

The phenomenon of jet break-up due to capillary instability has been extensively studied recently since its use in ink jet printing and soldering in electronic packaging. Rayleigh [12] first developed a linear stability theory to study the jet break-up phenomenon. Weber [13] improved Rayleigh's linear theory to include the viscosity effect and ambient medium. The theoretical predictions of Weber [13] appear to be in good agreement with the experiments of Donnelly and Glaberson [14]. McCarthy and Molloy [15] studied the correlation between the nozzle shape and issuing jet shape. Orme and Muntz [16] focused on the droplet stream of high directionality by using perturbation modulation. Chun and Passow [11] studied both droplet forming and solidification behavior using a charging ring to avoid droplet collision.

The hydrodynamic forces at the jet-medium interface enhance the growth rate of a disturbance and lead to a nonlinear relationship between jet breakup length and velocity. Since, under certain conditions, the linear theory may overestimate the aerodynamic effect, Sterling and Sleicher [17] developed a semi-empirical modification to Weber's theory to yield a good agreement with experimental data. Reitz [18] proposed a numerical modification of the linear theory and generated curve-fits for the maximum growth rate of the disturbance. In this section, Reitz's solution is used to assess the accuracy of Weber's solution for the operating range considered in the present droplet generator.

Growth Rate of Disturbance. Based on Weber's theory, the disturbance growth rate (β) which includes the effects of the viscosity and ambient medium, is governed by:

$$\beta^2+\frac{12\mu\gamma^2}{\rho_j d_j^2}\beta=\frac{4\sigma}{\rho_j d_j^3}(1-\gamma^2)\gamma^2+\frac{2U_j^2\rho_m\gamma^3K_0(\gamma)}{\rho_j d_j^2K_1(\gamma)} \qquad (1)$$

where $K_n(\gamma)$ is a modified Bessel function of the first kind of order n (where $n=0$ or 1); d_j is the jet diameter; μ, ρ_j, and σ are the viscosity, density, and surface tension of the jet fluid, respectively; U_j is the jet velocity; ρ_m is the density of the ambient medium; and γ is the dimensionless wave number equal to $\pi d_j/\lambda$. Here λ is the wavelength of the disturbance as shown in Fig. 2. In the above equation, it has been assumed that an initial

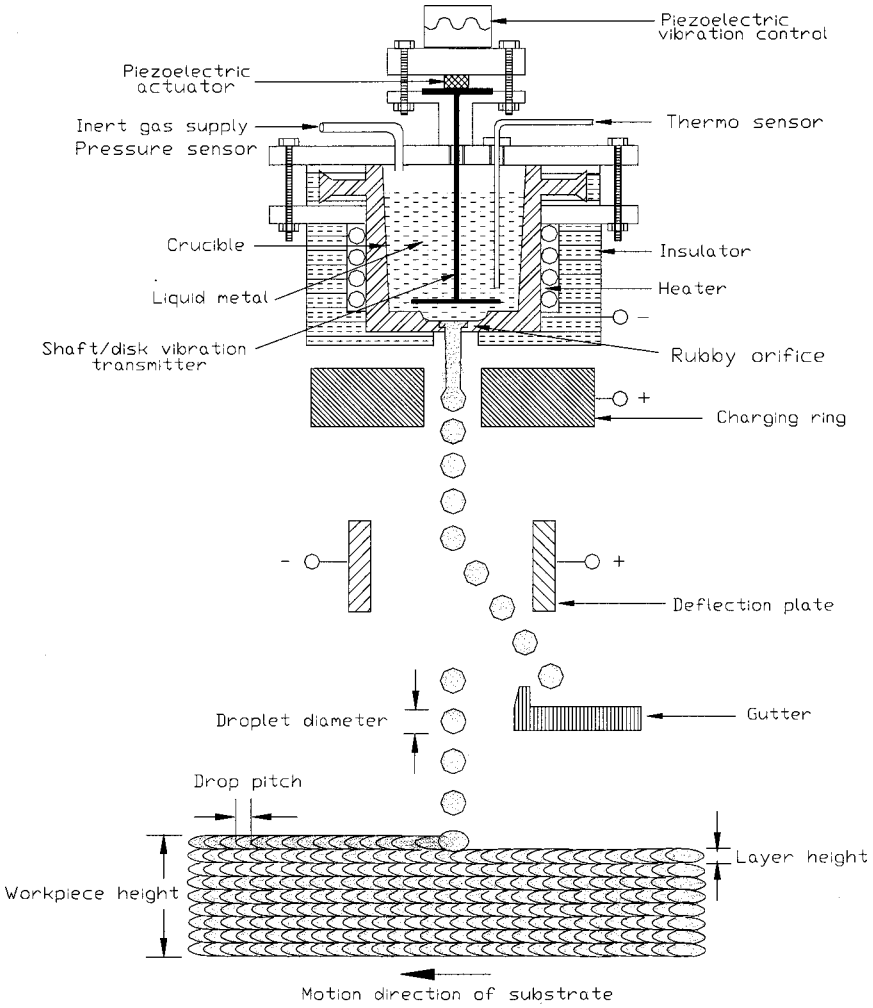

Fig. 1 Schematic diagram of droplet deposition system

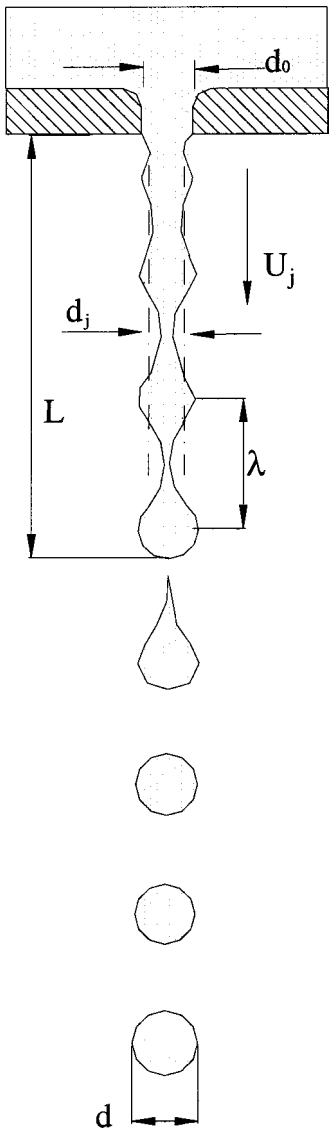

Fig. 2 Formation of droplets

infinitesimal disturbance of a given frequency grows in time t as $e^{\beta t}$ along the jet surface. The jet will break up when the amplitude of the disturbance is equal to the average jet radius, $d_j/2$. The disturbance growth rate (β) is a function of the wave number (γ); the jet becomes unstable when the wave number is less than 1.

Rearranging the above equation results in the following dimensionless quadratic equation:

$$\beta^{*2} + 12\ \mathrm{Oh}\ \gamma^2\beta^* = 4(1-\gamma^2)\gamma^2 + 2\gamma^3\frac{K_0(\gamma)}{K_1(\gamma)}\mathrm{We}_m^2 \qquad (2)$$

where β^* is the dimensionless growth rate of perturbation equal to $\beta/(\sigma/\rho_j d_j^3)^{0.5}$; **Oh** is the jet Ohnesorge number equal to $\mu/(\sigma\rho_j d_j)^{0.5}$, $\mathbf{We}_m$ is the Weber number of the ambient medium equal to $\rho_m U^2 d_j/\sigma$.

By solving the above equation, the relationship between the dimensionless growth rate and wave number can be obtained and is shown in Fig. 3 at various **Oh** and $\mathbf{We}_m$ numbers. The **Oh** number is a measure of the effect of the viscosity with respect to the surface tension. The Weber number is the ratio of the dynamic force and the surface tension. In general, the lower the **Oh** number or the higher the $\mathbf{We}_m$ number, the higher the growth rate. It can be restated that the ambient medium and the surface tension are

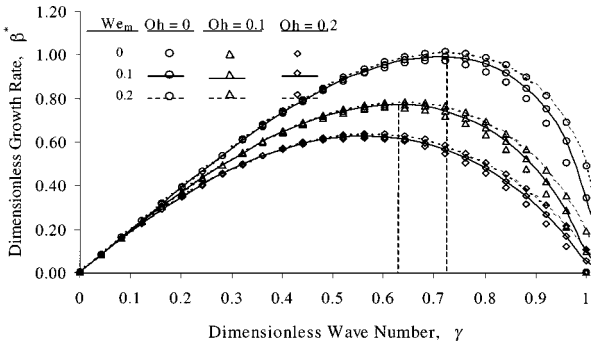

Fig. 3 Relationship between normalized growth rate and normalized wave number at various Ohnesorge and ambient Weber numbers

favorable for forming the droplet or enhancing the jet instability. The figure also reveals that an increase of viscosity has attenuation effects on the disturbances.

One can also observe that there exists a maximum growth rate for each curve shown in Fig. 3. The wave number corresponding to the maximum growth rate is called the optimal wave number (γ_{opt}). As shown, the lower the **Oh** number or the higher the $\mathbf{We}_m$ number, the higher the γ_{opt} number. However, for $\mathrm{We}_m < 0.1$, the change in γ_{opt} is negligible, i.e., less than 5 percent. Also, the optimal wave number decreases when the **Oh** number or viscosity decreases. For example, at $\mathbf{We}_m = 0$, the optimal wave number shifts to 0.62 from 0.72 when the **Oh** number varies from 0 to 0.1. This phenomenon results from the fact that high frequency (or low wavelength) energy attenuates faster than that of low frequency. It is to be noted that the wave number is proportional to frequency, i.e., $\gamma = \pi d_j/\lambda = \pi d_j f/U_j$.

As mentioned earlier, the linear theory may overestimate the ambient effect. Reitz [18] proposed a numerical modification of the linear theory and generated curve-fits for the maximum growth rate of the disturbance. A comparison of the optimal wave numbers based on Reitz's results with Weber's predictions is shown in Table 1. As indicated, the results predicted by the linear theory agree very well with Reitz's predictions; for the conditions compared, the differences vary from 0 percent to 6 percent. In fact, Lin and Reitz [19] based on an extensive survey have concluded that the linear theory can reliably predict the optimal wave number (γ_{opt}), as long as the jet operates at the condition that the droplet diameter generated is of the same order of magnitude as the jet diameter. In the present droplet generator, the ratio of the droplet diameter to the jet diameter is indeed of the same order of magnitude. Consequently, Weber's predictions on the optimal wave number are sufficiently reliable for the operating range considered and an appropriate control strategy for the droplet generator can be simply developed based on the linear solutions without consideration of the nonlinear effects.

Table 1 Comparison of optimal wave numbers by Weber [13] and Reitz [18]

		Optimal wave number, γ_{opt}		
Oh	$\mathbf{We}_m$	Weber	Reitz	Difference
0.0	0.0	0.701	0.697	0.6
0.0	0.1	0.721	0.704	2.4
0.0	0.2	0.721	0.721	0.0
0.1	0.0	0.601	0.610	1.5
0.1	0.1	0.621	0.595	4.4
0.1	0.2	0.641	0.604	6.1
0.2	0.0	0.561	0.580	3.3
0.2	0.1	0.561	0.554	1.3
0.2	0.2	0.581	0.559	3.9

Table 2 Properties of materials and dimensionless numbers

Material	H_2O	Sn95/Sb5	Wax
Liquidus temperature (T_1) [°C]	0	240	63
Operating temperature (T_j) [°C]	20	257	68
Surface tension[1] (σ) [N/m]	0.073	0.5338	0.0289
Viscosity[1] (μ_j) [Pa·s]	1.07×10^{-3}	1.85×10^{-3}	6.19×10^{-3}
Liquid density[1] (ρ_j) [Kg/m^3]	998	6965	846
Solid density at 20°C[1] (ρ_s) [Kg/m^3]	⋯	7268	921
Reynolds number[2] ($\mathbf{Re}=\rho_j U_j d_j/\mu_j$)	699	2818	103
Weber number[2] ($\mathbf{We}_j=\rho_j U_j^2 d_j/\sigma$)	31	29	66
Ohnesorge number[2] ($\mathbf{Oh}=\mu_j/(\sigma\rho_j d_j)^{0.5}$)	7.93×10^{-3}	1.92×10^{-3}	7.29×10^{-2}
Normalized breakup length[3] (L_{opt}/d_j)	68	65	121
Normalized droplet diameter[3] (d_{opt}/d_j)	1.89	1.88	1.95
Normalized jet diameter[3] (d_j/d_0)	0.87	0.87	0.87
Air environment[3] (ρ_m/ρ_j)	1.16×10^{-3}	1.67×10^{-4}	1.37×10^{-3}
Nitrogen environment[3] (ρ_m/ρ_j)	1.12×10^{-3}	1.61×10^{-4}	1.33×10^{-3}
Helium environment[3] (ρ_m/ρ_j)	1.62×10^{-4}	2.33×10^{-5}	1.92×10^{-4}
Argon environment[3] (ρ_m/ρ_j)	1.66×10^{-3}	2.38×10^{-4}	1.96×10^{-3}
Ambient Weber number[3]			
$\mathbf{We}_m$ (Air)	3.56×10^{-2}	4.83×10^{-3}	9.04×10^{-2}
$\mathbf{We}_m$ (N_2)	3.44×10^{-2}	4.67×10^{-3}	8.79×10^{-2}
$\mathbf{We}_m$ (He)	4.97×10^{-3}	6.77×10^{-4}	1.27×10^{-3}
$\mathbf{We}_m$ (Ar)	5.09×10^{-2}	6.90×10^{-3}	12.94×10^{-2}

[1]Calculated operating temperature.
[2]Based on diameter $d_j=250$ [μm] and velocity $U_j=3.0$ [m/s].
[3]ρ_m is evaluated at the atmosphere condition.

Moreover, for a typical deposition condition for making water, wax, and tin droplets in a standard environment, the $\mathbf{We}_m$ number is less than 0.2 as indicated in Table 2. Consequently, the environmental effect can be neglected at normal environmental conditions. Also, the conditions selected in Table 2, the jet diameter is 250 μm and the jet velocity is 3 m/s, are consistent with the conditions selected by other investigators (Orme [20], Yim [21]). Without the environmental effect ($\mathbf{We}_m=0$), one can easily find the analytical expression for the optimal wave number: $\gamma_{opt}=1/[2(1+3\ \mathbf{Oh})]^{1/2}$.

Droplet Size. Based on data similar to those shown in Fig. 3, the optimal wave number (γ_{opt}) can be estimated by the given **Oh** and $\mathbf{We}_m$ numbers of a liquid. Using the relation of $f=U_j/\lambda$, the optimal perturbation frequency can be found as:

$$f_{opt}=\gamma_{opt}U_j/\pi d_j \tag{3}$$

The diameter of the droplet (d) at the optimal condition can be determined by the use of mass conservation, i.e., the mass of the cylindrical jet section prior to the breakup of the jet is equal to that of the spherical droplet, $\pi d_j^2\lambda/4=\pi d^3/6$, namely:

$$d/d_j=(1.5\pi/\gamma)^{1/3}=(1.5U_j/d_j f)^{1/3} \tag{4}$$

The droplet diameter (d) in the above equation is based on the density at the liquid temperature. However, the droplet size is normally measured at the room temperature and volume shrinkage occurs during solidification as well as a temperature decrease. To account for the shrinkage effect, the final solidified droplet diameter (d_s) can be obtained by considering the change in density from the jet temperature to the measurement temperature:

$$d_s/d_j=(1.5\pi\rho_j/\gamma\rho_s)^{1/3}=[1.5\rho_j U_j/(\rho_s d_j f)]^{1/3} \tag{5}$$

where ρ_s is the density at the measurement temperature. Substituting the wave number in Eq. (5) by the optimal wave number, one can obtain the optimal droplet diameter (d_{opt}) expressed by the optimal wave number as well as the optimal perturbation frequency:

$$d_{opt}/d_j=(1.5\pi\rho_j/\gamma_{opt}\rho_s)^{1/3}=[1.5\rho_j U_j/(\rho_s d_j f_{opt})]^{1/3} \tag{6}$$

Figure 4 shows that the normalized optimal diameter, d_{opt}/d_j as a function of **Oh** number at different $\mathbf{We}_m$ numbers. As shown, two distinguishable regions can be found. For an **Oh** number larger than 0.01, the droplet diameter increases monotonically as the **Oh** number increases; for an **Oh** number less than 0.01, the normalized d_{opt}/d_j is almost constant at approximately 1.9 for $\mathbf{We}_m=0$. Since the **Oh** number is much smaller than 0.01 for the deposition of molten metal droplets (as shown in Table 1 for tin), the optimal droplet diameter can be assumed to be 1.9 times of the jet diameter. Also, because the optimal wave number γ_{opt} shifts to larger values as the $\mathbf{We}_m$ number increases, and in turn, the d_{opt}/d_j decreases. The normalized diameter d_{opt}/d_j changes approximately 7 percent as the $\mathbf{We}_m$ increases from 0 to 1.0.

It should be noted that the jet diameter d_j can be directly controlled by the nozzle diameter d_0. Based on the conservation of mass and momentum, Harmon [22] obtained a closed form solution for ideal fluids such that the jet diameter is equal to 0.87 of the nozzle diameter and the jet velocity (U_j) is equal to 1.33 times of the nozzle velocity (U_0). Middleman and Gavis [23] conducted experiments for three different liquids and their observation agreed with Harmon's prediction for the condition where the jet Reynolds number ($\rho_j U_j d_j/\mu$) larger than 100. For a Reynolds number less than 100, the ratio (d_j/d_0) gradually increases to

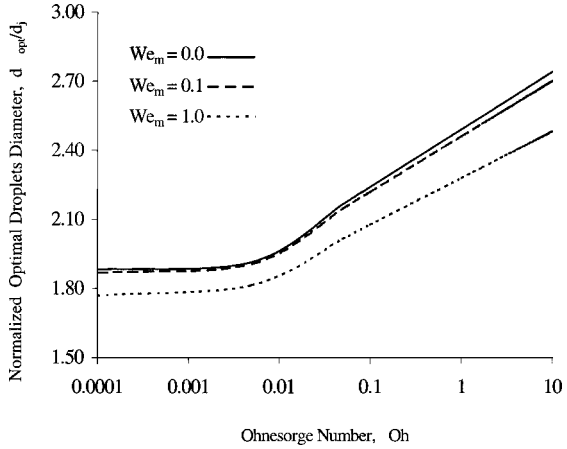

Fig. 4 Normalized optimal droplet diameter versus Ohnesorge number at various ambient Weber numbers

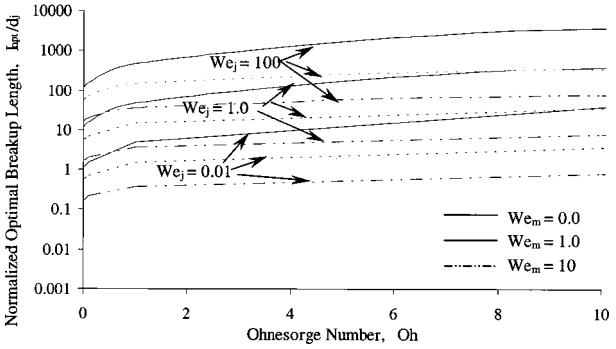

Fig. 5 Normalized optimal break-up length versus Ohnesorge number at various jet Weber numbers

1.12 as the **Re** approaches zero. In the present experiment, the **Re** is between 2750 and 3450 for tin alloy and between 64 and 130 for wax. For the cases of **Re** from 64 to 100, the ratio (d_j/d_0) decreases linearly from 0.9 to 0.87 and (U_j/U_0) increases proportionally from 1.23 to 1.33 following the data reported by Middleman and Gavis [23].

Breakup Length. Information on the break-up length of a jet is imperative for designing the charging device for a freeform fabrication system (Fig. 1). According to the linear stability theory, a jet will break up when a neck on the surface of the jet contracts to zero or the disturbance $\delta = \delta_i e^{\beta t}$ grows to the jet radius $d_j/2$, where δ_i is an initial infinitesimal perturbation. As mentioned earlier, the growth rate (β) becomes a maximum, i.e., β_{opt}, at the optimal wave number (γ_{opt}). If τ is the time required to break up the jet at the maximum growth rate, it can be calculated from $d_j/2 = \delta_i \exp(\beta_{\text{opt}}\tau)$. Thus, the optimal break-up length (L_{opt}) of the jet can be obtained from the jet velocity (U_j):

$$L_{\text{opt}} = \tau U_j = U_j \ln(d_j/2\delta_i)/\beta_{\text{opt}} \tag{7}$$

It is to be noted that ''infinitesimal'' is a mathematical description and cannot be precisely defined. Clift et al. [24] estimated the initial perturbation, δ_i, to be 0.1 percent of the jet diameter for most of engineering applications. Many experiments have been made to study the break-up length. Based on an intensive review, McCarthy and Molloy [15] found that the break-up length decreases as the amplitude of disturbance increases and the logarithmic term, $\ln(d_j/2\delta_i)$, could be assumed to be 12 when the Reynolds number is less than about 1000. Rewriting Eq. (7) into a dimensionless form,

$$\frac{L_{\text{opt}}}{d_j} = \frac{12\ \text{We}_j^{0.5}}{\beta^*_{\text{opt}}} \tag{8}$$

where $\mathbf{We}_j = \rho_j U_j^2 d_j/\sigma$ is the jet Weber number. Results of the above equation are depicted in Fig. 6, where the maximum growth rate, β_{opt}, can be obtained by Eq. (1) or by data shown in Fig. 3. The dimensionless optimal breakup length, L_{opt}/d_j is plotted against the Ohnesorge number at various $\mathbf{We}_j$ and $\mathbf{We}_m$. As shown, the break-up length grows gently as the **Oh** increases. However, the effect of $\mathbf{We}_j$ on the break-up length is much larger. As shown, the break-up length increases almost proportionally with $\mathbf{We}_j$, i.e., the faster the jet velocity the longer the break-up length. Figure 5 also shows that the break-up length decreases with an increase of $\mathbf{We}_m$. This implies that the ambient pressure can diminish the break-up length because the disturbance becomes more rapid when the $\mathbf{We}_m$ increases, as indicated in Fig. 3.

Testing Apparatus

Based on the formulation and consequent deposition guidelines presented in the preceding sections, a uniform droplet deposition system was designed and constructed as shown Fig. 6. The corresponding major components of the generator are schematically shown in Fig. 1 and include a crucible, piezoelectric oscillator, electromagnetic droplet selection system, controllable substrate, and PC controller. The crucible, electromagnetic droplet selection system, and controllable substrate are housed in a deposition chamber that is environmentally controlled, mainly to prevent oxidation of the droplets. In this section, the apparatus is described and the operation of the apparatus is discussed. Results from experiments conducted with this laboratory scale apparatus are presented over a wide range of operating conditions.

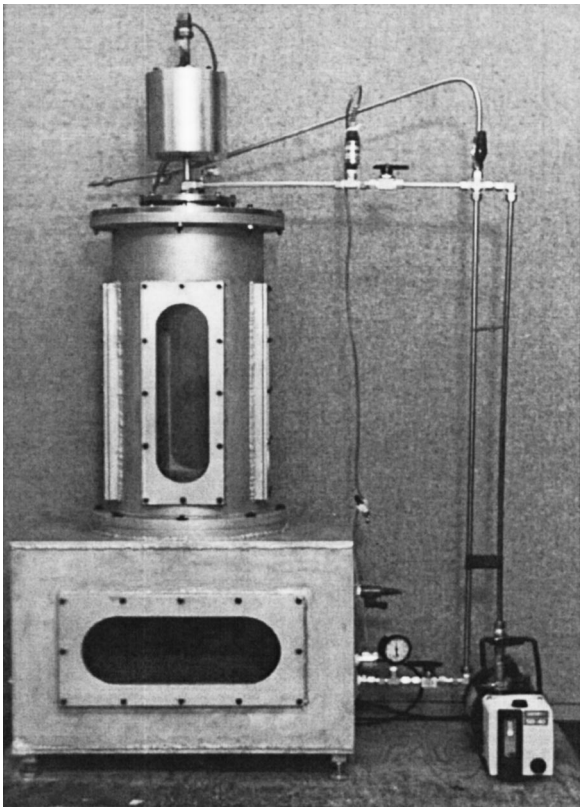

Fig. 6 Experimental droplet deposition system

Major Components. The crucible is made of a stainless-steel coated with chromium and designed to be heated up to 1000°C by a resistant heating device. The heated crucible holds and liquifies a charge of the forming material. The electromagnetic droplet selection system is comprised of a modulated circular charged electrode, a constant voltage deflection plate, and a stationery gutter. The semi-molten metal droplet generated is only deposited to the location where the object or structure is to be built. For a location where no object needs to be formed, the unwanted droplet must be discarded. For an unwanted droplet, electric charge is loaded by the modulated electrode. While the droplets are passing through the deflection system, only the charged or unwanted droplets are deflected and intercepted by the gutter for recycling as shown in Fig. 1. If the droplet is not charged it will land vertically to build the desired shape. The position substrate is centered on a motorized stage capable of translating the substrate in all three Cartesian axes with micrometer resolution.

The metal part is built layer-by-layer from the bottom up in sequential order as guided by computer software until it is completed. The piezoelectric oscillator, modulated charge electrode, and position controllable substrate are all synchronized and controlled by the PC controller. Inputs from the computer to the system are governed by a software which accepts three dimensional data in CAD-type formats, slices the data into appropriate layers and then properly positions the substrate beneath the uncharged

droplet to form each layer. This approach is similar to most commercially available layer-based systems (Beaman et al. [2]).

Operation and Testing. The liquified material is ejected through a nozzle located at the bottom of the heated crucible to form a jet. The jet is subjected to force disturbances at a frequency between 1 kHz and 50 kHz imposed by the piezoelectric driven oscillator inside the crucible. As discussed earlier, under this regulated disturbance, the jet is broken up into a stream of small droplets. In fact, the relationship among the droplet diameter, the jet diameter, and the wavelength of the disturbance (or the wave number) can be found in Eq. (5). The desired or uncharged droplets are then deposited on a specific location controlled by the motorized substrate. The height between the nozzle and the substrate could be controlled in order to meet the required solidification and fabrication conditions.

The ejection pressure needed to control the jet velocity is obtained from a pressurized nitrogen tank. A gas reservoir is installed between the crucible and the gas tank to dampen the fluctuation of pressure in the system. Experiments were first conducted to obtain the relationship between the ejection pressure (ΔP) and the nozzle velocity (U_0). Two types of materials: a tin-antimony alloy (Sn95-Sb5) and a paraffin wax are selected for the experiments. These two materials are also used for the evaluation of the droplet quality and its landing accuracy.

For each experiment, the ejection pressure is held constant and the amount of the flow ejected and the associated time are recorded. By providing the specific weight or density of the liquified material, the corresponding nozzle velocity can be estimated. Two different nozzle diameters (d_0): 203 and 254 μm, were considered. The dimensions of the crucible used are shown in Fig. 7, where d_1 and d_2 are the diameters of the crucible and base, respectively, and equal 1.5- and 100-mm; h_0, h_1, and h_2 are the elevation heads and are equal to 0.25-, 4.75-, and 100-mm, respectively.

The correlation between the nozzle velocity and the ejection pressure for three sets of experimental conditions is plotted in Fig. 8. As shown, the experimental results are also compared with the analytical predictions. For both the paraffin-wax and tin-alloy cases, the experimental results agree excellently within 6 percent with the analytical prediction for the conditions considered. Consequently, the experimental results can be concluded to be very reliable and were adopted to correlate between the ejection pressure and nozzle velocity in the present study.

The analytical solution used in comparison in Fig. 8 is obtained based on the principle of energy conservation (Fox and McDonald [25]):

$$U_0 = \frac{-A + [A^2 + 4(\Delta P + B)C]^{1/2}}{2C} \tag{9}$$

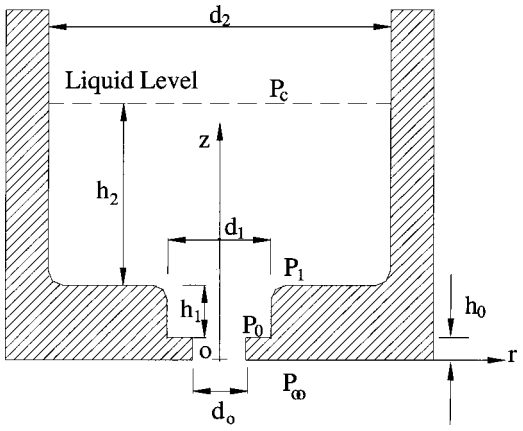

Fig. 7 Crucible geometry

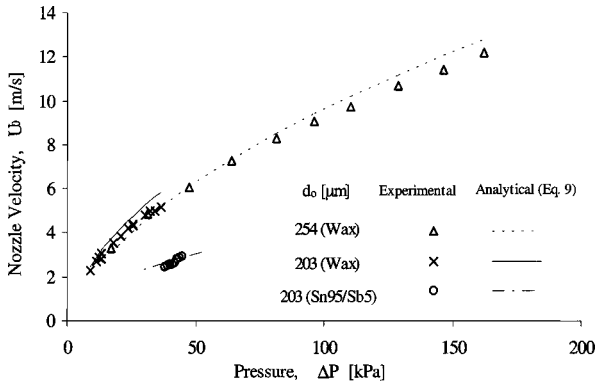

Fig. 8 Relationship between nozzle velocity and ejection pressure

where U_0 is the nozzle velocity and ΔP is the ejection pressure or the difference between the crucible pressure (P_c) and the ambient pressure (P_∞) as shown in Fig. 7. The flow constants, *A*, *B*, and *C*, in the above equation can be found as:

$$A = 32\mu_j \rho_j d_0^2 \left(\frac{h_0}{d_0^4} + \frac{h_1}{d_1^4} + \frac{h_2}{d_2^4} \right) \tag{10}$$

$$B = \rho_j g (h_0 + h_1 + h_2) \tag{11}$$

and

$$C = \rho_j [\alpha_0 + K_0 + K_1 (d_0/d_1)^4]/2 \tag{12}$$

where α_0 is the kinetic energy coefficient which is dependent on the velocity profile in the nozzle section; K_0 and K_1 are the loss coefficients for the sudden contraction from diameter d_1 to d_0 and from diameter d_2 to d_1, respectively; and g is the gravity acceleration. Since the velocity profile at the entrance region is quite flat, a power-law profile having the seventh power is assumed for the velocity at the nozzle. Following the formula provided by Fox and McDonald [25], the kinetic energy coefficient, α_0, is found to be 1.05. Also based on the geometry of the present crucible design and the correlation provided by Fox and McDonald [25], the loss coefficients, K_0 and K_1, are found to be 0.48 and 0.5, respectively. In the above formulation, the pressure head losses due to the viscous effects in the nozzle have been taken into account. The material properties of μ_j and ρ_j can be found from Table 2.

Experiment and Results

The quality of the fabricated part is dependent on the ability to produce uniform size droplets as well as to control the landing position or flight direction of the droplets. As a result, the purpose of the present experiment is to specifically evaluate the uniformity of the droplets generated as well as the landing accuracy of these droplets. A tin-antimony alloy (Sn95-Sb5) and American paraffin wax with a melting point of 63°C are selected for the evaluation; two nozzle diameters, 203 and 254 μm, were used. For the experiment, the wax was melted to 68°C or 5°C higher than the melting temperature, while the Sn95-Sb5 was heated to 257°C. The melted material was then ejected and subjected to force disturbances at an imposed frequency in order to form a stream of droplets. To measure the droplet diameter, a water bucket is placed under the nozzle approximately 1.5 m to allow the droplet having enough flying time to be solidified. For wax, the droplets are solidified in an open-air environment, while for the tin alloy, a nitrogen environment is imposed.

Materials Properties. The corresponding material properties for both the wax and Sn95-Sb5 alloy in the liquid phase are summarized in Table 2. The density (ρ), surface tension (σ), or vis-

Table 3 Physical properties used for estimation of Sn95-Sb5 and wax

Metal	Sn	Sb	Sn95-Sb5[1]	Wax
Liquidus temperature [K]	505	904	513	336
Solid density at 20°C (ρ_s) [kg/m^3][1]	7300	6650	7268	921
Density at liquidus point (ρ_m) [kg/m^3]	7000	6483	6975	856
Density coefficient ($d\rho/dT$) [kg/m^{3}K]	-0.6127	-0.5650	-0.610	-2.1
Viscosity at liquidus point (μ_m) [Pa·s]	1.94×10^{-3}	1.45×10^{-3}	1.92×10^{-3}	6.6×10^{-3}
Viscosity coefficient ($d\mu/dT$) [Pa·s/K]	-4.0×10^{-6}	-1.8×10^{-6}	-3.9×10^{-6}	-8.28×10^{-5}
Surface tension at liquidus point (σ_m) [N/m]	0.544	0.367	0.535	2.93×10^{-2}
Surface tension coefficient ($d\sigma/dT$) [N/mK]	-7.0×10^{-5}	-5.0×10^{-5}	-6.9×10^{-5}	-8.0×10^{-5}

[1]Estimated based on data for Sn and Sb.
[2]Calculated from data.

cosity (μ) at the operating temperature (T) are linearly extrapolated from the data based on the melting temperature (T_m):

$$X = X_m + (T - T_m)(dX/dT) \tag{13}$$

where X is the density, surface tension, or viscosity at the operating temperature, X_m is the density (ρ_m), surface tension (σ_m), or viscosity (μ_m) at the melting temperature, and dX/dT is the density coefficient ($d\rho/dT$), surface tension coefficient ($d\sigma/dT$), or viscosity coefficient ($d\mu/dT$).

All the data used to predict the properties at the operating temperature are summarized in Table 3. For tin and antimony, the values of ρ_m, σ_m, $d\rho/dT$, and $d\sigma/dT$ can be found from the reference book by Brandes and Brook [26]. The viscosity (μ_m) and viscosity coefficient ($d\mu/dT$) at the melting temperature are linearly extrapolated from the data provided by Manko [27]. The estimated viscosities of Sn and Sb at the melting point are within the range reported by Wittenberg and Ofte [28]. From Eq. (13), the density (ρ) and surface tension (σ) and viscosity (μ) at the operating temperature can be calculated. Densities for the materials at room temperature are directly obtained from Boyer and Gall [29]. Finally, the properties of Sn95-Sb5 reported in Table 2 are based on the properties of two individual constituencies, tin and antimony, and combined in proportion to their respective atomic weight fractions.

The wax properties reported in Table 2 were estimated by using Eq. (13). The density and viscosity data needed in the estimation at the melting temperature can be found from Warth [30] for an American paraffin wax having a melting temperature at 63°C. The surface tension data of the wax at the melting temperature is based on the data by Gao and Sonin [31]. The water properties in Table 2 were directly obtained from Incropera and DeWitt [32]. All the data used in the property calculations for Sn95-Sb5 and American paraffin wax in Table 2 are summarized in Table 3.

Droplet Size Variation. The droplets generated in each testing frequency were collected with a bucket. The solidified droplets were first examined for their appearance and shape. Each droplet diameter was then measured using an optical microscope with the precision of 1 μm. The droplets produced at the optimal frequency can be found in Figs. 9 and 10 for the wax and tin-alloy cases, respectively. As shown in both figures, the droplets produced have a smooth surface and spherical shape. The wax droplets were produced using a nozzle diameter of 254 μm at a jet velocity and optimal frequency of 4.56 m/s and 3600 Hz, respectively, while the Sn95-Sb5 droplets were generated at 4200 Hz having a 203 μm nozzle diameter and 4.12 m/s jet velocity.

The variation of droplet size as a function of frequency is shown in Fig. 11 for making wax droplets at the jet diameter and velocity equal to 221 μm and 4.56 m/s, respectively. The diameter measurement at each frequency is obtained based on more than 100 samples. The mean and the corresponding range of standard deviation (Δ) are plotted in the figure. The theoretical prediction based on Eq. (5) is also shown in the figure. As indicated, the prediction of the droplet size agrees very well, within 4 percent,

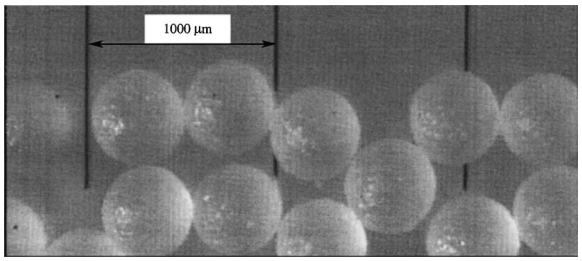

Fig. 9 Micrograph of wax droplets using 254-μm diameter nozzle

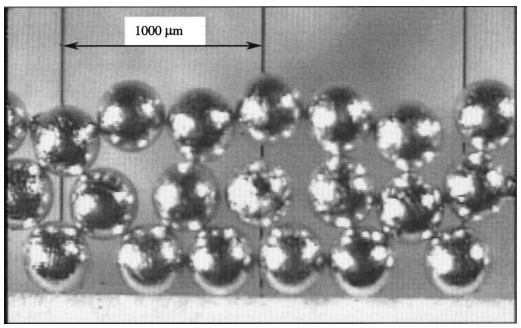

Fig. 10 Micrograph of Sn95-Sb5 droplets using 203-μm diameter nozzle

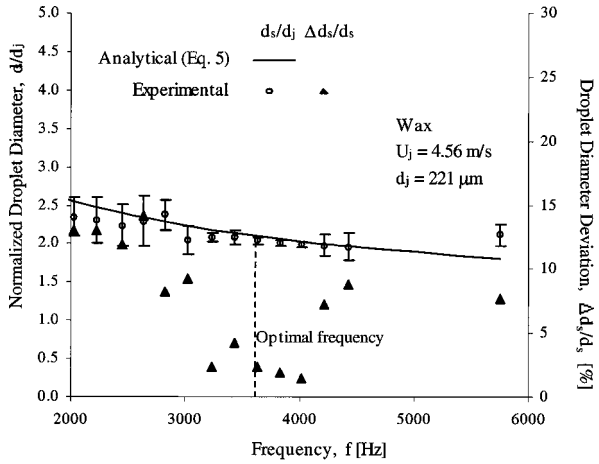

Fig. 11 Normalized wax droplet diameter and its deviation produced at 4.56-m/s jet velocity

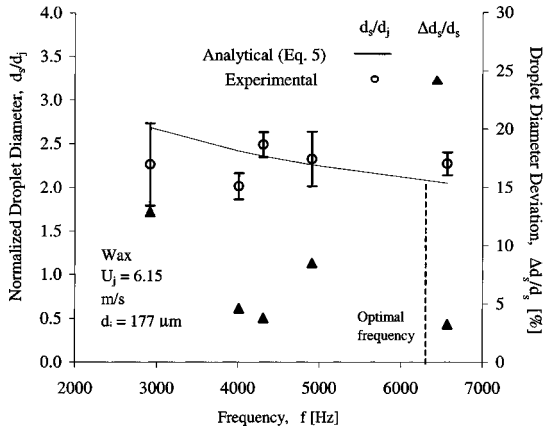

Fig. 12 Normalized wax droplet diameter and its deviation produced at 6.15-m/s jet velocity

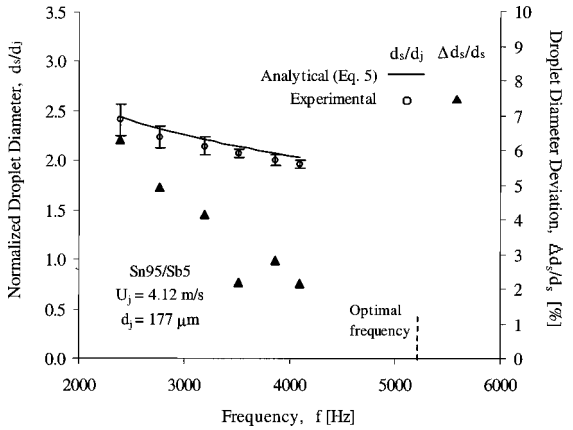

Fig. 14 Normalized Sn95-Sb5 droplet diameter and its deviation produced at 4.12-m/s jet velocity

with the mean measured value at the region near the optimal frequency; however, the calculation somewhat overestimates the measurement at lower frequencies and underestimates it at higher frequencies. It is also found that the discrepancy between the prediction and measurement decreases as the frequency approaches the optimal value (the dotted line in the figure). To evaluate the discrepancy, the normalized standard deviation ($\Delta d/d_s$) is also presented in the figure. As shown, the discrepancy changes from less than 3 percent for frequencies near the optimal value to more than 10 percent for frequencies away from the optimized one.

Figure 12 shows the results for the wax droplets, which are similar to those shown in Fig. 11, although the jet operates at a smaller diameter (177 μm) and higher jet velocity (6.15 m/s). Based on the five sets of data presented in Fig. 12, a similar conclusion can be found from the figure, i.e., the droplet size prediction agrees reasonably good with the actual measurement, and the minimum standard deviation ($\Delta d/d_s$) is located in the region near the optimal frequency.

Results for making tin-alloy droplets are shown in Figs. 13 and 14 for a jet velocity at 2.26 m/s and 4.12 m/s and jet diameter of 203 μm and 177 μm, respectively. Again, less than 3 percent of the normalized standard deviation ($\Delta d_s/d_s$) is observed at frequencies approaching the optimized value. In droplet size variations, the theoretical results based on Eq. (5) agree very well with the experimental results. As shown, except data at frequency of 1785 Hz, the equation prediction is consistent with the measured values within 6 percent for a jet speed at 2.26 m/s; for a jet speed at 4.12 m/s, the prediction agrees with the measurement better than 3 percent.

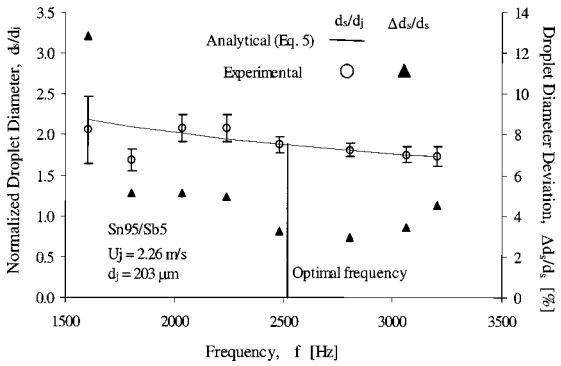

Fig. 13 Normalized Sn95-Sb5 droplet diameter and its deviation produced at 2.26-m/s jet velocity

The main reason that the experimental results near the optimal frequency reach a maximum in size consistency is somewhat complex. After carefully examining the size distribution of the droplet samples produced at each frequency, it is found that those measurements whose mean value agrees well with the theoretical prediction have a variation close to the normal distribution, but those droplets whose average value does not agree well with the theoretical prediction have an irregular distribution. This fact seems to imply that many other frequencies other than the applied frequency may exist in the input signal. Although in the experiment, only a single sinusoidal frequency is applied, this sinusoidal frequency is generally composed of a fundamental mode at the applied frequency and many minor modes at different frequencies. Also, the other frequency may simply be the noise frequency induced by the instrument or background during the experiment. If the growth rate of the jet disturbance at the other frequencies is at the same level of the applied frequency, the jet may simply break up at the other frequency. Accordingly, the droplet size generated is different from those generated at the applied frequency. For the applied frequency near the optimal region, the growth rate should be much bigger than those of the other frequencies. Consequently, the jet can be broken up much faster to form the droplets by the applied frequency than by the other frequencies, which is the main reason more uniform droplets are generated at the region near the optimal frequency or at the highest growth rate.

Moreover, as shown in Fig. 3, the variation of the growth rate is more moderate at a higher Ohnesorge number. As a consequence of this, the growth rate at the other frequencies may have a higher probability to have the same level of growth rates as that of the applied frequency. In our case, the Ohnesorge number for the wax case is larger than 0.2 and that for the tin-alloy case is less than 0.002. This could be the reason why the results for the tin-alloy case are better than those for wax, because the growth rate variation of a wax jet is much more moderate than that for a tin-alloy jet.

Droplet Deposition. A stream of Sn95-Sb5 droplets generated is shown in Fig. 15 using a 203-mm diameter nozzle at a nozzle velocity of 2.5 m/s and a disturbance frequency of 2510 Hz; this is a typical occurrence which is observed in all experiments for both wax and tin droplets. The droplets can be observed to be very round, uniform, and evenly spaced. Also, as shown the droplets are aligned into a straight line. This implies that the droplets are all moving in the same direction at the same speed, which is one of the basic requirements for a good droplet deposition system for freeform fabrication. It is to be noted that since some of the droplets are electrically charged, a certain degree of repulsion forces are generated among them. As a result, the system,

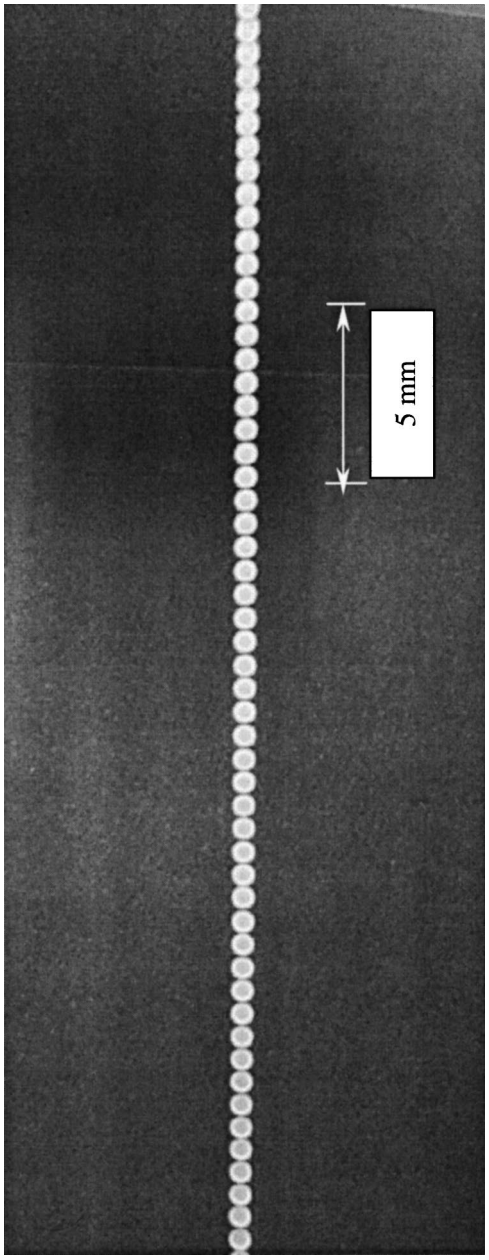

Fig. 15 Stream of Sn95/Sb5 droplets using 203-μm diameter nozzle

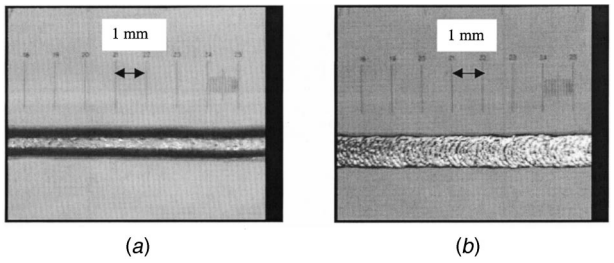

Fig. 16 Top and bottom views of deposited Sn95/Sb5 layer at 0.10-m/s substrate velocity

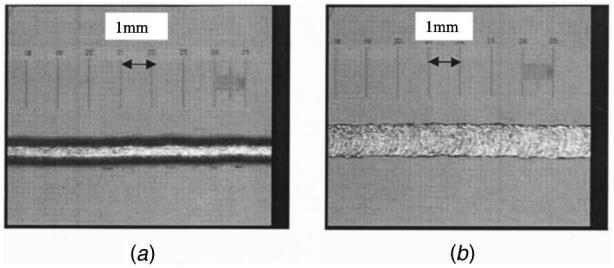

Fig. 17 Top and bottom views of deposited Sn95/Sb5 layer at 0.18-m/s substrate velocity

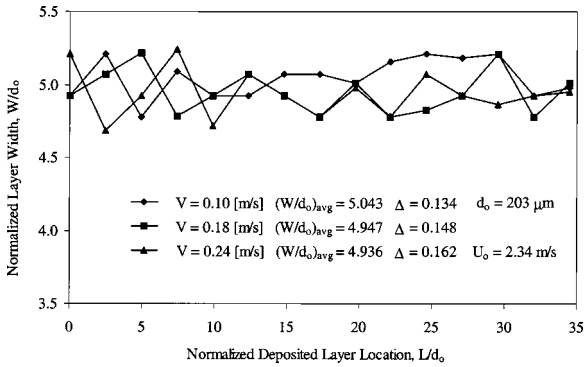

Fig. 18 Normalized width deviation of deposited Sn95/Sb5 layer

especially the charging electrode or device, has to be carefully designed. Otherwise, it may be difficult to keep the flying droplets in a straight trajectory (Yim [21]).

In the deposition experiments, the stream of droplets was deposited onto a moving glass substrate which was placed 45 mm below the nozzle to allow the droplet to have an adequate length of flying time to be partially solidified. The droplets were fully solidified on the substrate to form a layer. Figures 16 and 17 show the Sn95-Sb5 layers solidified at the moving substrate at speeds of 0.1 and 0.18 m/s, respectively. Both the top and bottom views are shown in the figures which were taken from an optical microscope with a resolution of 1 μm. Since the droplets were deposited onto a glass substrate, the bottom view can be easily recorded. The droplets were generated using a 203-μm diameter nozzle at 2.34 m/s nozzle velocity; the crucible or operating temperature was 530 K with the ambient temperature at 294 K. The straightness of the deposited layer is examined using a reference line in the optical microscope. The central line along the nominal width agrees very well with the reference line within its resolution limit of 1 μm. In fact, a linear regression analysis is conducted to correlate fifteen selected locations along the central line of the deposited layer, the resulted correlation coefficient to a straight line is 0.99 which is an excellent number. The coefficient always lies between -1 and $+1$. It is zero when the two coordinates of the fifteen selected locations are totally independent of one another, while it reaches 1 when the two coordinates correlate perfectly, i.e., no deviation from a straight line.

Also, the width of the deposited layer is measured and its deviation was calculated. Figure 18 shows the variation of the layer width for three layers made at substrate speeds (V) of 0.1, 0.18, and 0.24 m/s. The layers examined are 7 mm long and fifteen measurements were taken and the nozzle diameter (d_0) of 203 μm was used for normalization. As shown, the standard deviations (Δ) of the layer width are 0.134, 0.148, and 0.162 for the normalized average width of 5.043, 4.947, and 4.936. This is equivalent to approximately 3 percent variation of the average layer width. This can be translated to the dimension precision of the product fabricated by the droplet deposition technique to be at

3 percent of the nominal dimension of the product without any post-treatment. Therefore, the present technique has a great potential to be used for making precision parts. Based on the results discussed above, it has also been demonstrated that the flight direction and the landing position of the droplets can both be controlled within a few percentages of the droplet size.

Concluding Remarks

The theory of generating droplets for freeform fabrication of metal components has been examined. Appropriate formulas based on the linear stability theory for liquid jets have been developed for the design and operation of a droplet deposition system. The magnitude of the ambient effect has been specifically quantified by the ambient Weber number and particularly interesting as compared with other parameters in the development of those formulas. Following the theoretical results obtained, a droplet generator is designed and built to make wax and tin alloy droplets. Experiments have been conducted at a wide range of jet velocities, frequencies, and droplet sizes. Experimental results have reasonably agreed with the formulas developed. Theoretical analyses and experimental results qualitatively prove that the Ohnesorge number is more dominant than the ambient Weber number for the conditions considered.

The relationship between the input frequency and the droplets generated is specifically investigated. Low droplet size deviation was observed around the optimal frequency. The reason for better size uniformity and agreement between the prediction and measurement values at frequencies near the optimal value is also discussed. Using the optimal frequency, the droplet sizes can be controlled having a size deviation of less than 3 percent. The present study also indicates that using the droplets generated at the optimal frequency for deposition, the variation of the deposited layer can be managed within 3 percent of its width for the specific condition considered. Also, it has been found that the increase of the perturbation amplitude, which helps to advance the signal/noise ratio, improves the uniformity of the droplets generated in the range of frequencies considered.

Since the droplet variation and landing accuracy produced by the present system can be controlled within 3 percent of its diameter or deposited width satisfy the requirements of electronic packaging, the sophisticated and expensive feedback control system can be indeed avoided (Rocha [33], Lovelady and Watts [9]). Also, the present system can handle higher melting point materials at high volume production rate which are also the primarily requirements for the next generation fine pitch packaging technologies.

In conclusion, operating at the optimal frequency is recommended, because it not only produces more uniform droplets but also shortens the time and distance for forming the droplets and in turn, increases the overall productivity. Moreover, shortening the break-up length allows for a shorter deposition chamber which results in better control of the landing position and the dimensions of the deposited layer, as well as being able to utilize a smaller piece of apparatus to reduce equipment space and costs.

Acknowledgments

The authors gratefully acknowledge the support of this research by the U.S. National Science Foundation under grant no. DMI-9696062 and DMI-9812984 and by the 1997 Innovative Concepts Program of the Department of Energy through Battelle Pacific Northwest National Laboratory under award no. 310470-A-U4. The authors would also like to thank Professor Jung-Hoon Chun of the Massachusetts Institute of Technology, Professor E. Dan Hirleman of Purdue University, and Professor Timothy W. Tong of Colorado State University for their support during the conduct of this work.

Nomenclature

A, B, C = flow constants defined in Eqs. (10)–(12), respectively
d = diameter or droplet diameter
f = frequency of perturbation
h = elevation head
K = loss coefficient
L = breakup length or traveling length
Oh = Ohnesorge number, $\mu_j/(\sigma\rho_j d_j)^{0.5}$
P = pressure
Re = Reynolds number, $\rho_j U_j d_j/\mu_j$
t = time
U = velocity
V = substrate velocity
We = Weber number, $\rho_j U^2 d_j/\sigma$
α = kinetic energy coefficient
β = growth rate of perturbation
β^* = normalized growth rate
δ = perturbation amplitude
γ = dimensionless wave number, $\pi d_j/\lambda$
λ = wavelength
μ = viscosity
ρ = density
σ = surface tension
τ = break-up time
Δ = standard deviation

Subscript

i = initial
j = jet
m = ambient
0 = nozzle
opt = optimal
s = solid or solidified
0,1,2, = section 0,1,2, . . .

References

[1] Jacobs, P. F., 1996, *Stereolithography and Other BP&M Technologies*, Society of Manufacturing Engineers, Dearborn, MI.
[2] Beaman, J. J., Barlow, J. W., Bourell, D. L., Crawford, R. H., Marcus, H. L., and McAlea, K. P., 1997, *Solid Freeform Fabrication: A New Direction in Manufacturing*, Kluwer Academic, Boston, MA.
[3] Orme, M., Huang, C., and Courter, J., 1996, ''Precision Droplet-Based Manufacturing and Material Synthesis: Fluid Dynamics and Thermal Control Issues,'' Atomization Sprays, **6**, pp. 305–329.
[4] Kuhn, L., and Myers, R. A., 1979, ''Ink-Jet Printing,'' Sci. Am., **240**, No. 4, Apr., pp. 162–178.
[5] Wallace, D. B., 1989, ''Automated Electronic Circuit Manufacturing Using Ink-Jet Technology,'' ASME J. Electron. Packag., **111**, pp. 108–111.
[6] Lau, J., 1995, *Ball Grid Array Technology*, McGraw-Hill, New York.
[7] Hayes, D. J., Wallace, D. B., Boldman, M. T., and Marusak, R. M., 1994, ''Picoliter Solder Droplet Dispensing,'' Int. J. Microcirc. Electron. Packag., **16**, pp. 173–180.
[8] Ju, T. H., Lin, W., Lee, Y. C., and Liu, J. J., 1994, ''Effects of Ceramic Ball-Grid-Array Package's Manufacturing Variations on Solder Joint Reliability,'' ASME J. Electron. Packag., **116**, pp. 242–248.
[9] Lovelady, M. L., and Watts, J. D., 1999, ''Closed Loop Feedback for Continuous Mode Materials Jetting,'' *24 IEEE/CPMT Int. Electronics Manufacturing Technology Symposium*, IEEE, pp. 189–195.
[10] Lee, H. C., 1974, ''Drop Formation in a Liquid Jet,'' IBM J. Res. Develop., **18**, pp. 173–180.
[11] Chun, J., and Passow, C. H., 1993, ''Production of Charged Uniformly Sized Metal Droplets,'' U. S. Patent 5,266,098.
[12] Rayleigh, J. W. S., 1878, ''On the Stability of Jets,'' Proc. London Math. Soc., **10**, pp. 4–13.
[13] Weber, C., 1931, ''The Decomposition of a Liquid Jet,'' Z. Angew. Math. Mech., **11**, pp. 136–154.
[14] Donnelly, R. J., and Glaberson, W., 1966, ''Experimental on the Capillary Instability of a Liquid Jet,'' Proc. R. Soc. London, Ser. A, **290**, pp. 547–556.
[15] McCarthy, M. J., and Molloy, N. A., 1974, ''Review of Stability of Liquid Jets and the Influence of Nozzle Design,'' Chem. Eng. J., **7**, pp. 1–20.
[16] Orme, M., and Muntz, E. P., 1987, ''New Technique for Producing Highly Uniform Droplet Streams over an Extended Range of Disturbance Wave Number,'' Rev. Sci. Instrum., **58**, pp. 279–284.
[17] Sterling, A. M., and Sleicher, C. A., 1975, ''The Instability of Capillary Jets,'' J. Fluid Mech., **68**, pp. 477–495.

[18] Reitz, R. D., 1987, ''Modeling Atomization Processes in High-pressure Vaporizing Sprays,'' Atom. Spray Technol., **3**, pp. 309–337.
[19] Lin, S. P., and Reitz, R. D., 1998, ''Drop and Spray Formation from a Liquid Jet,'' Annu. Rev. Fluid Mech., **30**, pp. 85–105.
[20] Orme, M., 1994, ''Rapid Solidification Materials Synthesis with Nano-Liter Droplets,'' SAE Trans. J. Aerospace, **102**, pp. 1876–1881.
[21] Yim, P. W., 1996, ''The Role of Surface Oxidation in the Break-up of Laminar Liquid Metal Jets,'' Ph.D. thesis, M.I.T, Cambridge, MA.
[22] Harmon, Jr., D. B., 1955, ''Drop Sizes from Low Speed Jets,'' J. Franklin Inst., **259**, pp. 519–523.
[23] Middleman, S., and Gavis, J., 1961, ''Expansion and Contraction of Capillary Jets of Newtonian Liquids,'' Phys. Fluids, **4**, No. 3, pp. 355–359.
[24] Clift, R., Grace J. R., and Weber, M. E., 1978, *Bubble, Drops and Particles*, Academic, New York, pp. 333–340.
[25] Fox, R. W., and McDonald, A. T., 1985, *Introduction to Fluid Mechanics*, Wiley, New York, pp. 356–373.
[26] Brandes, E. A., and Brook, G. B., ed., 1992, *Smithells Metals Reference Book*, Section 14.2, Butterworth-Heinemann, Oxford, England.
[27] Manko, H. H., 1979, *Solders and Soldering*, McGraw-Hill, New York, pp. 120–121.
[28] Wittenberg, L. J., and Ofte, D., 1970, ''Viscosity of Liquid Metals,'' *Physicochemical Measurements in Metals Research*, Part 2, R. A. Rapp, ed., Wiley, New York.
[29] Boyer, H. E., and Gall, T. L., ed., 1985, *Metals Handbook*, Desk Ed., American Society for Metals, Metal Park, OH, pp. 1.46–1.49.
[30] Warth, A. H., 1956, *The Chemistry and Technology of Waxes*, Reinhold, New York, NY.
[31] Gao, F. Q., and Sonin, A. A., 1994, ''Precise Deposition of Molten Microdrops: the Physics of Digital Microfabrication,'' Proc. R. Soc. London, Ser. A, **444**, pp. 533–554.
[32] Incropera, F. P., and DeWitt, D. P., 1985, *Fundamentals of Heat and Mass Transfer*, 2nd ed., Wiley, New York, pp. 774–775.
[33] Rocha, J. C., 1997, ''Control of the UDS Process for the Production of Solder Balls for BGA Electronics Packaging,'' S.M. thesis, Massachusetts Institute of Technology, Cambridge, MA.